Energy Conversion and Management 197 (2019) 111865

Contents lists available at ScienceDirect

Energy Conversion and Management

journal homepage: www.elsevier.com/locate/enconman

Seasonal variation on the performance of the dry cooled supercritical CO_2 recompression cycle

M. Monjurul Ehsan*, Sam Duniam, Zhiqiang Guan, Hal Gurgenci, Alexander Klimenko

School of Mechanical and Mining Engineering, The University of Queensland, Brisbane, QLD 4072, Australia

ARTICLE INFO

Keywords:
Recompression cycle
Seasonal variation
Dry cooling
Supercritical CO_2
Thermal performance
Cooling tower

ABSTRACT

The dry cooling unit is integrated with a 25 MW recompression super-critical CO_2 (sCO_2) cycle for solar energy application. Based on the optimal operating condition, a natural draft dry cooling tower (NDDCT) is modelled for an ambient temperature of 20 °C and sCO_2 inlet condition of 67 °C and 7.96 MPa. The Kroger's detailed working principle of NDDCT is adapted in the simulation processes. The sCO_2 property variation with the change of bulk temperature is considered while modelling the heat exchanger unit inside the tower. The draft equation of the tower is solved by including various air-flow resistances at different parts of the tower. The heat input to the cycle is assumed to be supplied by the solar field with sufficient capacity of thermal storage. The seasonal effect on the performance of a dry-cooled sCO_2 recompression cycle is performed in Alice Spring, NT, Australia by using the daily meteorological data. The daily net power generation fluctuates in the range of 2.4% to 22.4% of the design value for the consecutive days. The year-round mean net power generation is 24.66 MW which corresponds to 50.9% cycle efficiency. The weekly and monthly seasonal variation of the plant performance in summer, autumn, winter, and spring is performed based on the mean maximum and minimum temperature data. The mean net power produced in summer and winter is 22.9 MW and 26.4 MW respectively. The fluctuation of heat input to the cycle, heat rejected by the cycle and air mass flow rate in NDDCT are demonstrated. Seven performance indicators (Thermal efficiency, exergetic performance criteria, exergy efficiency, maximum available work, ecological coefficient of performance, cooling efficiency, and ecological function criteria) are determined to evaluate the plant performance for the period of 1941 to 2018 using the mean temperature data.

1. Introduction

The globalization and rapid industrial development have intensified the necessity to substitute the perishable fossil fuel resources with renewable technologies [1]. In concentrated solar power (CSP) various thermodynamic power cycles can be integrated with the solar energy for the production of electrical energy [2]. The sCO_2 Brayton cycle is one of the most efficient solar to thermal power conversion cycles and it offers higher cycle efficiency over the conventional steam cycles due to the simple plant layout and the compactness of the turbo-machineries and heat exchangers [3,4]. An efficient cooling system is essential to deliver the required cooling tower exit temperature for maximum cycle efficiency [5]. The high-fluid density, higher isobaric heat capacity and lower specific volume of sCO_2 can considerably reduce the total compression work of the cycle [6]. Dry cooling is receiving noteworthy consideration over the wet cooling system due to the scarceness of fresh water source and the environmental concerns [7,8]. The dry cooling unit is mostly suited for CSP application due to its low operation and maintenance cost without fresh water consumption [9,10]. To maximize the sCO_2 cycle power plant efficiency, the cooling of sCO_2 is carried out in the vicinity of pseudocritical temperature and the change of sCO_2 thermodynamic properties with bulk temperature needs to be addressed in the heat exchanger [11,12]. This unique heat transfer mechanism of sCO_2 is different from the constant property fluids and requires additional consideration in designing the heat exchanger within the cooling tower [13].

Ma et al. [14] investigated the influence of main compression intercooling on the thermal performance of the recompression cycle. Deng et al. [15] performed the assessment of several CO_2 trans-critical cycles. Conboy et al. [16] tested a 1 MW simple sCO_2 Brayton cycle to experimentally assess the thermal performance as a function of turbine inlet conditions, the operating pressure ratio, and the mass flow rate. The experimental findings confirmed the potential of sCO_2 closed-loop Brayton cycles for large-scale power production. The cycle operated with a turbine inlet temperature of 342 °C, the pressure ratio of 1.65 and a mass flow rate of 2.7 kg/s. More recently, Wang et al. [17]

* Corresponding author.
E-mail address: m.ehsan@uqconnect.edu.au (M.M. Ehsan).

https://doi.org/10.1016/j.enconman.2019.111865
Received 25 April 2019; Received in revised form 25 June 2019; Accepted 21 July 2019
Available online 27 July 2019
0196-8904/

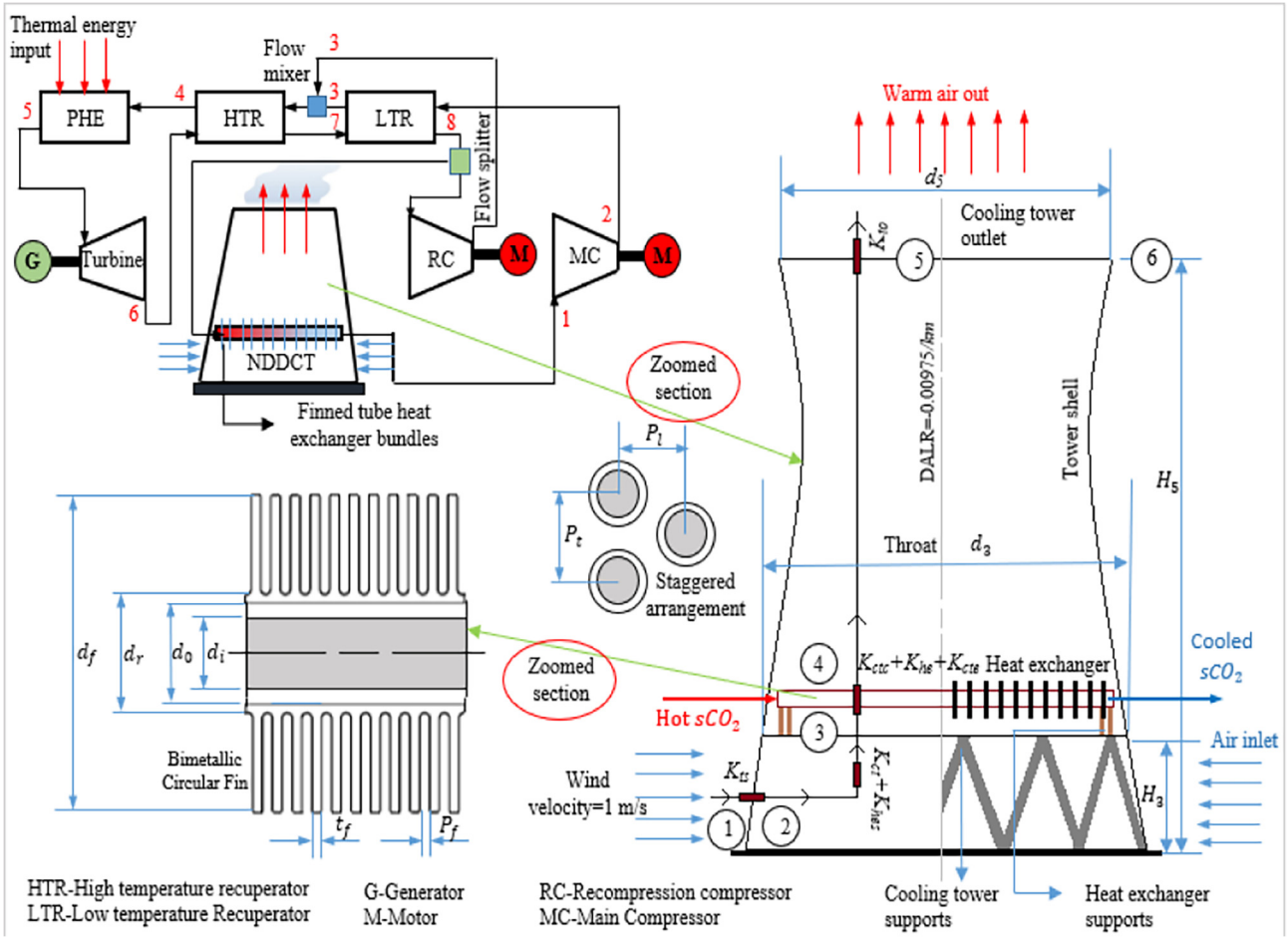

Fig. 1. The supercritical CO_2 cycle equipped with a detailed model of NDDCT.

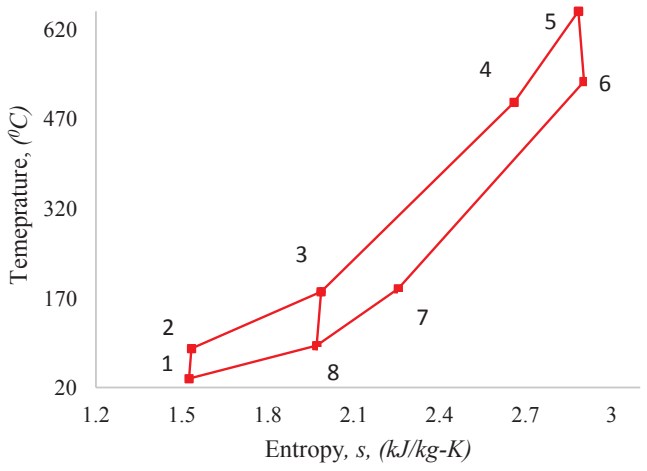

Fig. 2. T-s diagram of the recompression cycle.

performed the thermal performance (efficiency and specific work) of various layouts of sCO_2 cycles coupled with solar power towers using multi-objective optimization. Kim et al. [18] investigated the influence of the recuperator pinch point temperature difference on the sCO_2 recompression cycle performance. Luu et al. [19] conducted a dynamic analysis of the recompression cycle with variant levels of solar energy. Cheng at al. [20] performed the sensitivity analysis of the sCO_2 recompression cycle by optimizing the pressure ratio, split ratio and efficiency of the turbo-machineries.

Garg et al. [21] conducted a modelling study to investigate the advantages of the sCO_2 cycle over the steam cycle by assuming dry cooling. Turchi et al. [22] employed dry cooling to achieve a cycle efficiency of 50% with recompression cycle with reheat and intercooling. Iverson et al. [23] studied the dynamic response of the sCO_2 recompression cycle by varying the thermal input to the cycle and dry cooling was assumed. Persichilli et al. [24] highlighted the potential of sCO_2 in power cycles for larger-scale power production using the dry cooling system. Zeyghami and Khalili [25] examined the performance enhancement of air cooler using a daytime radiative cooler and the cycle efficiency of the recompression cycle increased by 5%. Padilla et al. [26,27] studied the influence of reheating and pressure drop of various sCO_2 power cycles (simple, recompression and recompression with main compression intercooling) using a dry cooler. Ho et al. [28] performed the economic analysis of sCO_2 cycle for CSP application and dry heat rejection was employed. Milani et al. [29] optimized the solar assisted sCO_2 cycle with air cooling, water cooling, and hybrid cooling mode by using Aspen heat exchanger package to design the air-cooling system. Li et al. [30] employed finned tube air cooler to conduct small-scale experimentation with the trans-critical CO_2 cycle. Luu et al. [31] performed the dynamic simulation of sCO_2 recompression cycle with air cooler as a heat rejection component.

The above studies paid emphasis mostly on the thermal performance and optimization of the power cycle. However, the detailed modelling of the finned tube heat exchanger unit was not presented or included for the analysis of the cooling tower. In their studies, the cooling component was treated as a black box with a prescribed cycle minimum temperature. However, recently a thermal analysis of various layouts of the dry cooling system conducted by adapting the detailed

Table 1
Energy equations for the recompression cycle.

Component	Equation
Turbine	$\eta_T = \frac{h_5 - h_6}{h_5 - h_{6s}}$, $W_T = M_s(h_5 - h_6)$
High-temperature recuperator, HTR	$h_4 - h_3 = h_6 - h_7$
Low-temperature recuperator, LTR	$h_7 - h_8 = SR(h_3 - h_2)$
Primary heat exchanger, PHE	$M_X(h_a - h_b) = M_s(h_5 - h_4)M_X$ is the mass flow of heat transfer fluid and h_a and h_b are the inlet and outlet enthalpies respectively.
Main compression compressor, MC	$\eta_{MC} = \frac{h_{2s} - h_1}{h_2 - h_1}$, $W_{MC} = SR.\ M_s(h_2 - h_1)$
Recompression compressor, RC	$\eta_{RC} = \frac{h_{3s} - h_8}{h_3 - h_8}$, $W_{RC} = (1 - SR)M_s(h_3 - h_8)$
Net power generation	$W_{net} = W_T - W_{MC} - W_{RC}$

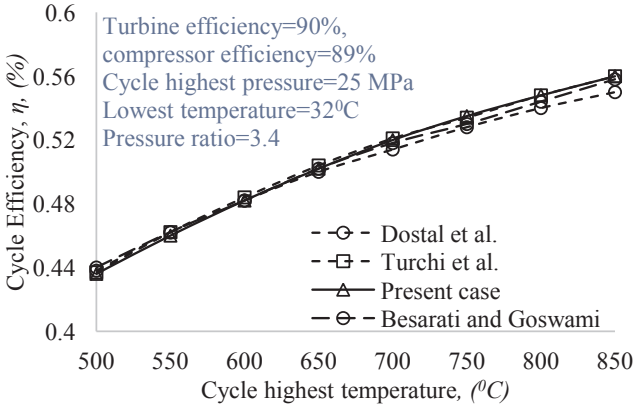

Fig. 3. Power cycle validation in terms of cycle efficiency against cycle highest temperature.

modelling approach [7]. Our previous work demonstrated the emphasis on the design of the cooling tower using MATLAB for direct and indirect configuration of the sCO_2 cooling system [10,32]. However, the tower was not integrated with the power cycle, and the influence of various cycle parameters on the cooling potential and cycle performance was not investigated. This work will explore this research gap by investigating the influence of cooling tower design strategy on cycle thermal performance integrated with the NDDCT with a detailed modelling approach.

Currently, the modelling of the cooling system is performed in the context of optimal system performance. The novelty of the present work is the investigation of thermal performance of a sCO_2 power cycle employing a dry cooling system using the meteorological data in Alice Spring, Australia for the period of 1941 to 2018. No study is found in the literature which investigates the seasonal performance variation of a dry-cooled super critical CO_2 power cycle with a comprehensive design approach of cooling component. The novelty also includes the daily power fluctuation and annual plant performance analysis over a

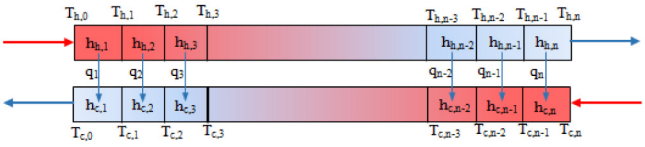

Fig. 5. Recuperator representation by discretizing into several segments.

wide range of environmental temperatures. The requirement of an efficient dry cooling system is to deliver an optimum tower outlet temperature for which the cycle offers the maximum efficiency. The NDDCT is equipped with power block and the thermal assessment of the NDDCT and cycle net power generation is analyzed over a wide range of ambient temperatures. The variation of heat input, heat rejected and the air mass flow rate is also investigated. The seasonal and annual variation of the plant performance is presented by evaluating various performance indicators using the historical temperature data.

2. Power cycle validation and modelling approach

Recompression sCO_2 cycle is considered and coupled with the NDDCT. In the recompression cycle, the pinch point problem is eliminated by two recuperators, as shown in Fig. 1. In comparison with regenerative Brayton cycle, it requires additional compressor and recuperator. It is efficient and has fewer blocks compared to other configuration of sCO_2 power cycles (partial cooling, split expansion, and main compression intercooling). For initial employment of sCO_2 power cycle on a large scale, the recompression cycle is the most promising candidates. The cycle T-s diagram is shown in Fig. 2. By splitting the flow after LTR, the heat capacity of the high-pressure stream side decreases and by setting the pinch point temperature constraint in the low-temperature recuperator to 5 °C, the pinch point problem is solved. The flow splitter at the exit of the low-pressure stream of LTR determines the amount of sCO_2 mass flowing into the cooling system. The remaining mass is pressurized by the RC and mixed with the outlet of the LTR. The heat input to the PHE varies to deliver the same cycle

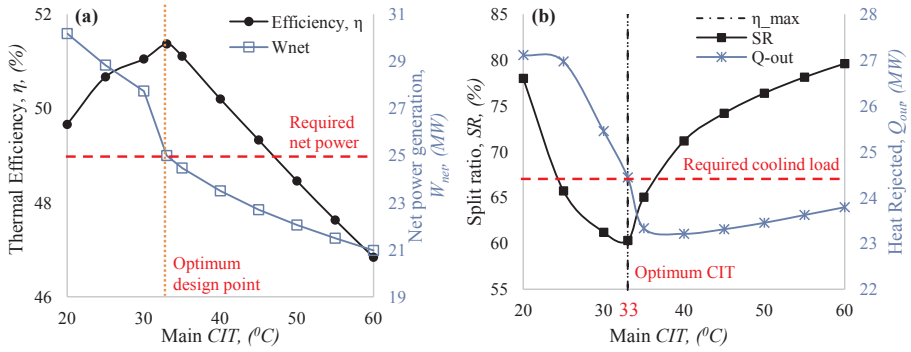

Fig. 4. Effect of main CIT on various cycle parameters to obtain the design condition for NDDCT modelling.

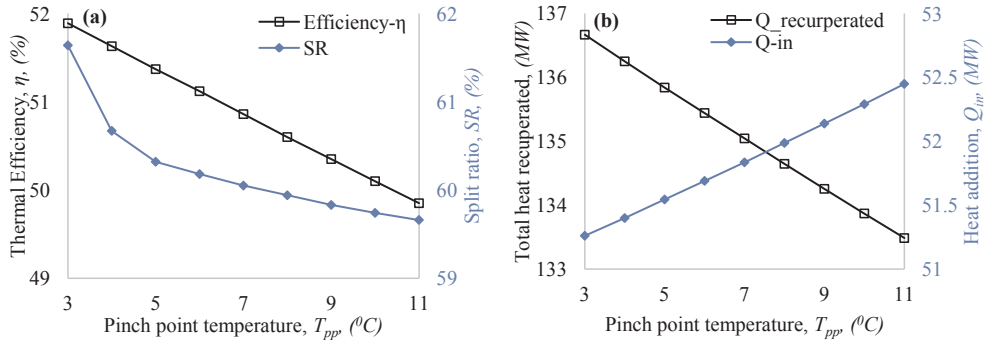

Fig. 6. Influence of pinch point temperature on (a) cycle efficiency and SR (b) heat transfer in recuperators and heat source heat exchanger.

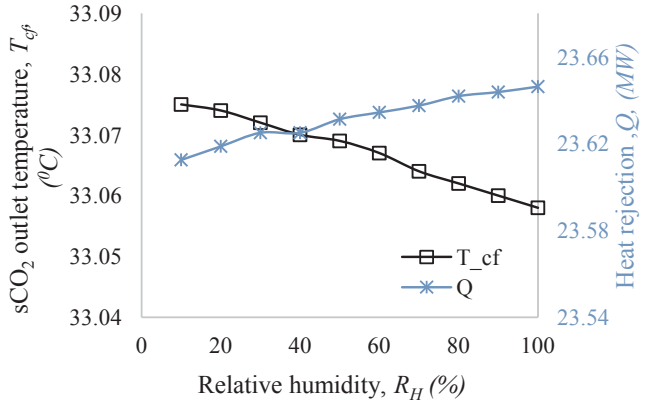

Fig. 7. Impact of relative humidity of air on cycle performance.

highest temperature at all working condition. The detail modelling of the heliostat field and solar receiver is beyond the scope. However, it is assumed that two thermal energy storage of sufficient capacity is able to provide the required heat to the power cycle to maintain a desired turbine inlet temperature. The cycle modelling is performed with a system simulation software IPSEpro [33].

The energy equations for various components of the recompression cycle are listed in Table 1. All the process attains a steady state condition. The heat loss due to radiation is assumed to be insignificant. The simulated results are validated in terms of cycle thermal efficiency with the variation of cycle highest temperature against the existing literature ([3,22], and [6]). The simulation result shows good agreement with literature as shown in Fig. 3. The boundary condition applied for the validation are kept the same as prescribed in the literature.

Table 2
Cycle input parameters for NDDCT and cycle modelling.

Parameter	Value
Net Power Generation	25 MW
Required heat rejection	23.8 MW
Isentropic efficiency of turbine	0.90
Isentropic efficiency of compressor	0.89
Mechanical efficiency	1.0
Turbine inlet temperature	650 °C
Compressor inlet temperature	33 °C
Split ratio	60%
Atmospheric air condition	20 °C, 1 m/s, 0.1 MPa
Air relative humidity	60%
Cycle maximum pressure	20 MPa
Compression ratio	2.5
Pinch point constraint	5 °C
Pressure drop in recuperators	20 kPa

3. Evaluation of optimal design condition

3.1. Optimum CIT and required cooling load

Preliminary assessment of the power cycle is conducted with a simple gas cooler model in order to rectify the optimum operating condition at which the NDDCT will be designed. The cooling tower will be designed based on the optimum main compressor inlet temperature determined from the preliminary analysis. Fig. 4(a) shows the variation of cycle thermal efficiency, η and net power generation, W_{net} with the increase of main CIT. The η is maximum at 33 °C due to the increase of specific heat and density of sCO_2 around the pseudocritical temperature. The W_{net} increases with lower CIT values. However, this comes in the cost of additional heat input in the PHE to deliver a cycle maximum temperature of 650 °C. Increasing the main CIT also changes the heat rejected by the cooling system, Q_{out} in the recompression cycle, as shown in Fig. 4(b). The Q_{out} initially drops with CIT and from CIT = 35 °C, the Q_{out} insignificantly increases from 23.3 MW to

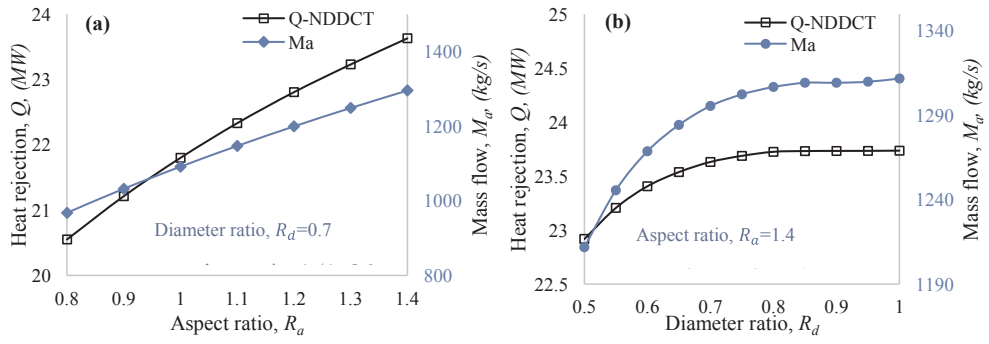

Fig. 8. Influence of (a) aspect ratio and (b) diameter ratio on tower performance.

Table 3
Model equations of NDDCT.

Parameter	Equation
Energy Equation	$Q = M_a C_{pa34}(T_{a4} - T_{a3}) = M_s C_s (T_{si} - T_{so}) Q = \frac{UAF_T[(T_{si} - T_{a4}) - (T_{so} - T_{a3})]}{\ln\left[\frac{(T_{si} - T_{a4})}{(T_{so} - T_{a3})}\right]}$ Here C_{pa34} and C_s represents air side specific heat measured with mean a temperature of heat exchanger and sCO_2 specific heat at constant pressure respectively. M_a and M_s are the mass flow of sCO_2 and air. Also, T_{a3} and T_{a4} are the air temperatures at the inlet and outlet of heat exchanger.
Overall thermal Conductance, *UA*	$UA = [\frac{1}{(h_s A_s)} + \frac{1}{2\pi k_t n_b n_{tb} L} ln\frac{d_o}{d_i} + \frac{1}{2\pi k_f n_b n_{tb} L} ln\frac{d_f}{d_o} + \frac{1}{(h_a e_f A_{aT})}]^{-1}$ Here, h_s and h_a are the heat transfer coefficient of sCO_2 and air side respectively, A_s and A_{at} are the surface area of sCO_2 and air side, e_f is the fin effectiveness, L is the length of finned tube, n_b is number of bundles, n_{tb} is the number of tubes in each bundle, and k_t and k_f are the thermal conductivity of tube side and fin side respectively. d_i, d_o, and d_f are the fins nomenclature shown is Fig. 1.
Temperature correction factor, F_T	$F_T = 1 - \sum_{i=1}^{4}\sum_{k=1}^{4} a_{i,k}(1-\varphi_3)^k \sin\left[2i arctan\left(\frac{\varphi_1}{\varphi_2}\right)\right]$ $\varphi_1 = \frac{(T_{si} - T_{so})}{(T_{si} - T_{a3})}; \varphi_2 = \frac{(T_{a4} - T_{a3})}{(T_{si} - T_{a3})}; \varphi_3 = \frac{(\varphi_1 - \varphi_2)}{\ln\left[\frac{(\varphi_1 - \varphi_2)}{(1-\varphi_2)/(1-\varphi_1)}\right]}$ Here, φ_1, φ_2, and φ_3 are dimensionless parameters and $a_{i,k}$ is the empirical constant evaluated from ref [34].
The overall effective air-side fin surface area, A_f	$A_f = n_r n_{tr} \frac{L}{P_f}\left[\pi\left\{\frac{2}{4}(d_f^2 - d_r^2) + d_f t_{fi}\right\}\right]$ Here, P_f is the fin pitch, and n_{tr} is the number of tubes in each row.
The exposed root area, A_r	$A_r = \pi n_r n_{tr} L d_r (P_f - t_f)/P_f$
Heat exchanger loss coefficient, K_{he}	$K_{he} = 31383.9475 Ry^{-0.332458} + \frac{2}{\sigma_a{}^2}\left(\frac{\rho_{a3} - \rho_{a4}}{\rho_{a3} + \rho_{a4}}\right)$ Characteristic Reynolds number, $Ry = \frac{M_a}{\mu_{a34} A_{frT}}$ Here, A_{frT} is the frontal area of heat exchanger.
Draft Equation	$p_{a1} - \left[p_{a5} + \frac{\left(\frac{M_a}{A_5}\right)^2}{2\rho_{a5}}\right] = (K_{ts} + K_{ct} + K_{hes} + K_{ctc} + K_{he} + K_{cte})\frac{\left(\frac{M_a}{A_{fr}}\right)^2}{2\rho_{a34}} + p_{a1}\left[1 - \left\{1 - 0.00975\frac{(H_3 + H_4)}{2T_{a1}}\right\}^{3.5}\right] + p_{a4}\left[1 - \left\{1 - 0.00975\left(H_5 - \frac{H_3}{2} - \frac{H_4}{2}\right)T_{a4}\right\}^{3.5}\right]$ Here, K_{ts}, K_{ct}, K_{hes}, K_{ctc}, K_{he}, K_{cte} are the air flow resistances in the tower. The correlations to measure these resistances are reported in ref [34]
sCO_2 heat transfer correlation [35]	$Nu_s = aRe_s{}^b Pr_s{}^c\left(\frac{\rho_{pc}}{\rho_s}\right)^n$ Here *a, b, c,* and *n* are the coefficients and ρ_{pc} and ρ_s are the densities of sCO_2 at bulk temperature and pseudocritical temperature respectively.

23.7 MW. The split ratio, *SR* initially decreases with the CIT. At CIT = 33 °C, the *SR* shows the lowest value at which the η is maximum. From CIT = 33 °C onwards, the *SR* starts increasing with the increase of CIT from 60.3% to 79.6%. Based on this analysis, the tower is required to model in which the tower exit temperature is close to 33 °C for optimal system performance.

3.2. Selection of pinch point temperature

The recuperators are discretized into several small heat exchanger segments for accurate measurement of heat transfer and temperature profile, as shown in Fig. 5. The LMTD method is employed in each segment to evaluate the local fluid properties for both high and low-pressure sides. This approach allows examining the local bulk temperature profiles for both sides of the recuperators. This approach also helps to examine the pinch point temperature along the recuperator length.

The influence of pinch point temperature, T_{pp} in the recuperator on the η is investigated in Fig. 6(a). Increasing the T_{pp} decreases the cycle *SR* from 51.8% to 49.8%. The lower the T_{pp}, the higher the η. The lower T_{pp} makes the heat exchanger more expensive and the higher T_{pp} yields more thermal losses. Hence, 5 °C is chosen as the optimum T_{pp}. In Fig. 6(b), it is seen that increasing the T_{pp} increases the heat addition to the PHE from 51.2 MW to 52.4 MW. The total heat recuperated in the HTR and LTR declines from 136.6 MW to 133.4 MW with the increase of T_{pp}.

3.3. Impact of relative humidity of air

The Fig. 7 shows the variation of air relative humidity has minimal impact on the sCO_2 outlet temperature and tower heat rejection. This nominal change will have an insignificant impact on the cycle thermal efficiency. Hence, the value of air humidity is taken as 60% to model the tower and perform the air temperature variation at various seasonal conditions. The daily mean temperature in Australia is around 20 °C, which is the design point air temperature to model the cooling system. A CSP plant would be running on stored heat as much as running on direct solar heat, therefore experiencing both the daytime and the nighttime temperatures. However, for a specific CSP location, this value should be changed accordingly and the tower should be designed based on the specified operating condition. It is a systematic procedure in modelling the dry cooling system and likewise, it is appropriate for other surrounding temperature values for designing the cooling tower.

3.4. Selection of geometric constraints of NDDCT

Prior to the modeling of NDDCT, the influence of various geometric parameters (aspect ratio, $R_a = H_5/d_3$ and diameter ratio, $R_d = d_5/d_3$) of NDDCT are investigated on the tower performance, as shown in Fig. 8. This tower geometric parameter analysis is performed in isolation with the power cycle. As expected, both the heat rejection and air mass flow in the tower increase proportionally with aspect ratio. However, there is an optimal value of R_d, since increasing the diameter ratio for a fixed aspect ratio increases the tower construction cost. Beyond $R_d = 0.7$, the heat dissipated by the tower and air mass flow show no significant variation, hence $R_d = 0.7$ is taken as the optimum diameter ratio. The

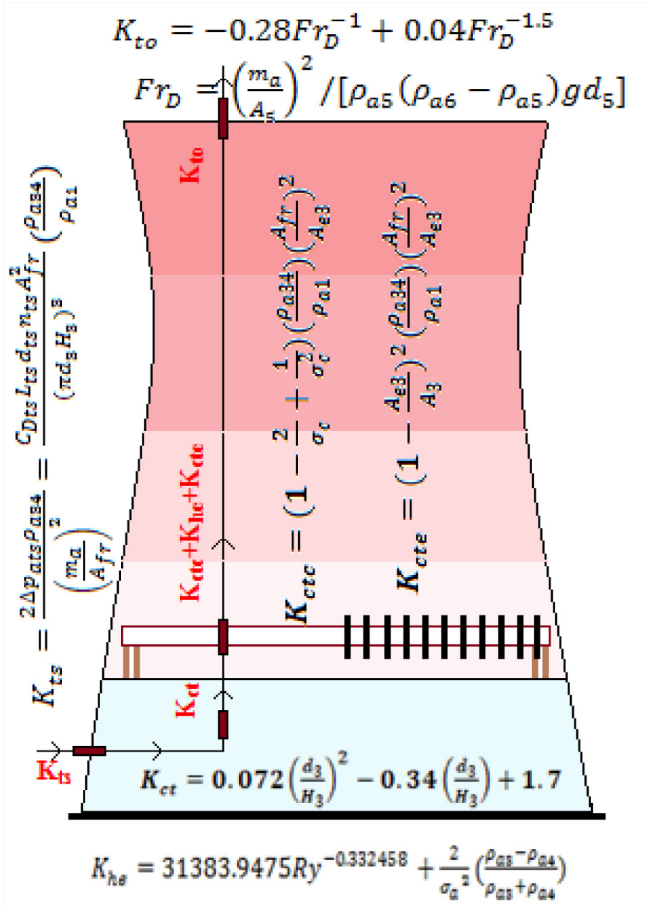

Fig. 9. Evaluation of various loss coefficients inside NDDCT.

Table 4
Required NDDCT specification.

Parameter	Value
Outlet height of tower, H_5	52.4 m
Unit height heat rejection	0.45 MW/m
Heat Exchanger height from ground, H_4	6 m
Inlet height of tower, H_3	5.7 m
Outlet tower diameter, d_5	26.2 m
Inlet tower diameter, d_3	37.4 m
Number of heat exchanger bundles, n_b	22
Average heat rejected by each bundle	1.08 MW
Number of tower supports: n_{ts}	27
Tower support dimension: *lts*	6.6 m
Frontal area of heat exchanger, A_{fr}	716 m^2
Air side surface area, A_a	0.53 × 10^6 m^2
Tube side surface area, A_t	3,924 m^2
Bare tube side surface area, A_{tb}	3310 m^2
Correction factor, F_T	0.94
Overall thermal conductance, *UA*	2159 kW/K
Characteristic air side Reynolds number, R_y	8,9849 m^{-1}
Average tube side Nusselt Number, *Nu*	2082
sCO_2 inlet velocity, V_s	0.95 m/s
sCO_2 outlet temperature, T_{so}	33 °C
Air outlet temperature, T_{a5}	40.7 °C

aspect ratio and frontal area ratios are taken as 1.4 and 0.65. The tower inlet height is calculated by $H_3 = d_3/6.5$ according to the Kroger's model [34]. The Support coefficient, C_{Dts} and width of tower support, d_{ts} are taken as 2 and 0.4 m respectively.

3.5. Boundary conditions for NDDCT modelling

The preliminary analysis shows that 33 °C is the design point compressor inlet temperature for attaining maximum cycle efficiency. Hence, the simple gas cooler model is replaced with detailed NDDCT model which is designed to cool the cycle fluid up to 33 °C in the heat exchanger. The cycle lower pressure (8 MPa) is kept above the critical pressure in order to maintain the supercritical state of the working fluid under all circumstances. The turbine inlet temperature is taken as 650 °C, as it is expected that the future CSP plants can attain such higher temperatures (580 °C to 750 °C) with the use of new novel molten salts. The boundary conditions to perform the integrated cycle simulation with NDDCT are prescribed in Table 2. The boundary conditions applied in components other than NDDCT are consistent with the existing literature. Most of the parameters are chosen from the existing literature, while few parameters (cycle mass flow, split ratio, and compressor inlet temperature) are optimized. Rest of the parameters are chosen based on an engineering design perspective.

4. NDDCT design procedure

The standard model of a cooling tower in IPSEpro does not consider the rapid property change of sCO_2 in the air-cooled heat exchanger. Hence, the model development kit (MDK) is used to model the NDDCT with model development language (MDL). With MDK, any component can be designed with a detailed modelling approach. The tower is modelled within the MDK and all other components are used as standard models for system simulation. Likewise, the programming language C++, the MDL is used to script the dry cooling model. The staggered arrangement of the tube is used for better thermal performance and fins are the type of bimetallic circular fin arranged transversely on the bare tubes. The geometry details of the heat exchanger are taken from ref [34]. The nodal approach takes account for the dramatic property change of sCO_2 with bulk temperature in the proximity of the pseudocritical region. The heat exchangers are discretized into small segments and the conventional LMTD method is employed in each segment for accurate prediction of local properties (heat transfer coefficient, bulk temperature, and fluid velocity). This mechanism allows visualizing the change of local parameters with a small change of bulk temperature along the tube length. The validation of the nodal approach performed in our previous research [10,32]. Table 3 shows the model equations of NDDCT used by MDL.

In MDK, the code starts solving the draft equation of the tower by measuring all the flow resistances at different parts of the tower, as shown in Fig. 9. The complete definition of these resistances is reported in ref [34]. The energy equations for both tube-side and air-side of the heat exchanger are solved with an initial estimation of heat exchanger bundles, cycle fluid outlet temperature, and air temperature at the outlet of the heat exchanger. The solution of the draft equation is the air mass flow. If the desired tower outlet temperature is not attained, the code at that time modifies the initial estimations and repeat the procedure. Finally, the code evaluates the required quantity of bundles and the tower specification for the accomplishment of 33 °C outlet temperature and cooling duty of 23.8 MW. The pinch point constraint is maintained during all iterations in the heat exchanger and cooling tower. Throughout each calculation, our code cautiously looks for any temperature cross-over. Table 4 displays the required cooling system specification which will be used for the analysis of cooling tower performance and power generation at different seasonal conditions.

5. Research output

The NDDCT thermal performance on a sCO_2 recompression cycle at various climate condition is investigated. The NDDCT is designed at 20 °C air temperature and sCO_2 inlet condition in the tower of 67 °C and 7.96 MPa. The NDDCT performance is analyzed over a wide range of

Table 5
Component-wise irreversibility equations of a recompression cycle.

Component	Equation
PHE	$I_{PHE} = [M_X(h_a - h_b) - T_{amb}(s_a - s_b)] - [M_s(h_4 - h_5) - T_{amb}(s_4 - s_5)]$ Here M_c and M_s are the mass flow of heat transfer fluid and working fluid respectively. T_{amb} represents the reference temperature.
HTR	$I_{HTR} = [M_s(h_6 - h_7) - T_{amb}(s_6 - s_7)] - [M_s(h_4 - h_3) - T_{amb}(s_4 - s_3)]$
LTR	$I_{LTR} = [M_s(h_7 - h_8) - T_{amb}(s_7 - s_8)] - SR[m_s(h_2 - h_3) - T_{amb}(s_2 - s_3)]$
NDDCT	$I_{NDDCT} = SR[M_s(h_8 - h_1) - T_{amb}(s_8 - s_1)] - [M_a(h_0 - h_i) - T_{amb}(s_o - s_i)]$
RC compressor	$I_{RC} = (1 - SR)W_{RC} - (1 - SR)[M_s(h_3 - h_8) - T_{amb}(s_3 - s_8)]W_{RC}$ is the power consumed by the RC compressor
MC compressor	$I_{MC} = SR.\ W_{MC} - SR[M_s(h_2 - h_1) - T_{amb}(s_2 - s_1)]W_{MC}$ is the power consumed by the MC compressor
Turbine	$I_{Turbine} = M_s[(h_5 - h_6) - T_{amb}(s_5 - s_6)] - W_T W_T$ is the power produced by the turbine.
Total Irreversibility	$I_T = I_{PHE} + I_{HTR} + I_{LTR} + I_{NDDCT} + I_{RC} + I_{MC} + I_{Turbine}$

Table 6
Cycle plant performance indicators of the proposed power plant.

Parameter	Equation
Thermal Efficiency, η	$\eta = \frac{W_{net}}{Q_{PHE}} Q_{PHE}$ is the heat input to the cycle and W_{net} is the net power generation
Exergy Efficiency, η_E	$\eta_E = \frac{W_{net}}{E_{in}} E_{in}$ is the exergy input to the cycle
Cooling Efficiency, η_C	$\eta_C = \frac{Range}{Range + Approach}$ Where, $Range = T_{si} - T_{so}$ and $Approach = T_{si} - T_{wetb}$. Here T_{si} and T_{so} are the sCO_2 inlet and outlet temperature and T_{wetb} is the wet bulb temperature
Ecological Function Criteria, *ECF*	$ECF = W_{net} - I_T$
Maximum Available Work, *MAW*	$MAW = E_{in} - I_T$
Ecological Coefficient of Performance, *ECOP*	$ECOP = \frac{W_{net}}{I_T}$
Exergetic Performance Criteria, *EPC*	$EPC = \frac{E_{in}}{I_T}$

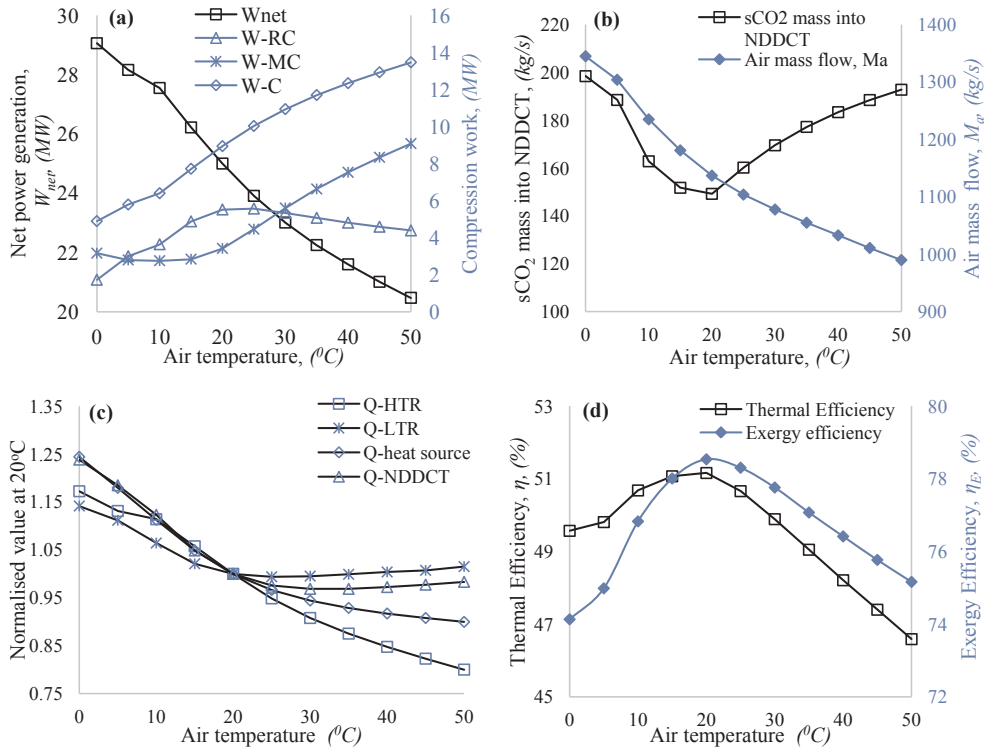

Fig. 10. Variation of (a) turbine and compressor work, (b) mass flow rate of two fluid streams inside the NDDCT, (c) energy transfer in the heat exchangers and NDDCT, and (d) exergy efficiency and thermal efficiency with air temperature.

ambient temperature. The variation of air temperature significantly impacts the performance of the tower which in turn influences the system performance due to the change of design point compressor inlet temperature. The turbo-machineries are modeled by defining their isentropic efficiencies consistent with the literature. The recuperators are discretized for accurate measurement of heat transfer with the evaluation of local properties (bulk temperature and local heat transfer coefficients). The thermodynamic variation of sCO_2 in these components are far away from the critical condition. However, the cooling process in NDDCT takes place where the thermodynamic property variation is dominant with the change of bulk temperature. At different seasonal conditions, the variation in the sCO_2 outlet temperature of

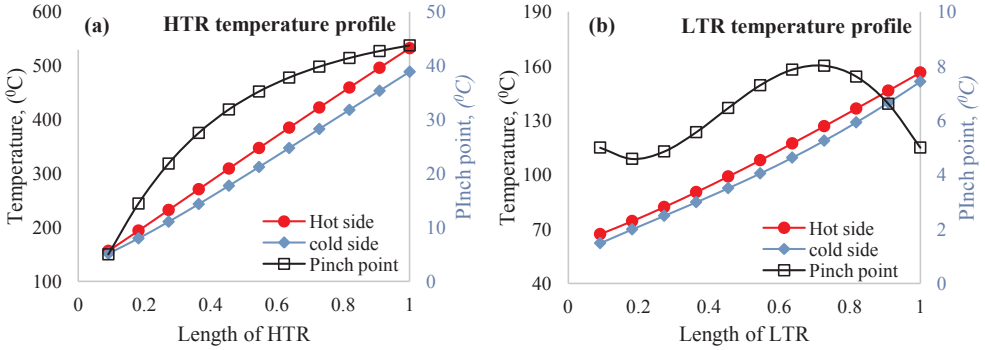

Fig. 11. Internal temperature profiles of hot side and cold side inside (a) HTR and (b) LTR.

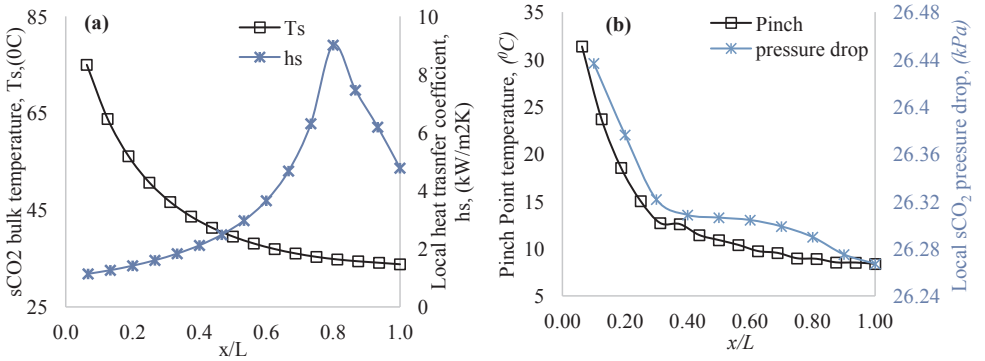

Fig. 12. (a) Variation of bulk temperature and local sCO_2 heat transfer coefficient, (b) pinch point and local sCO_2 pressure drop in the heat exchanger.

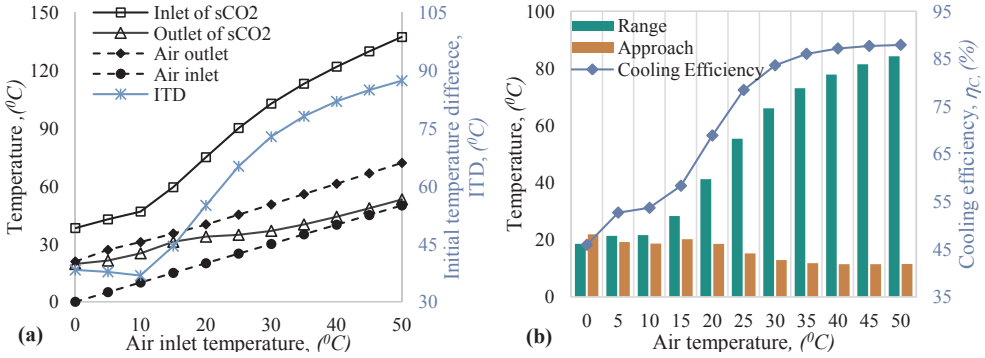

Fig. 13. (a) Temperature change of two fluid streams inside the NDDCT and (b) Evaluation of the cooling potential of NDDCT.

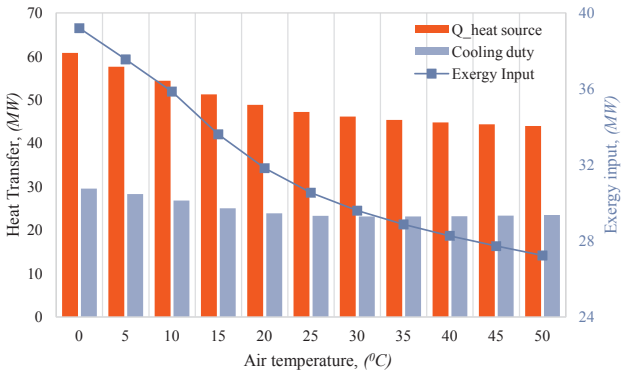

Fig. 14. Variation of heat addition, cooling duty and exergy destruction with air temperature.

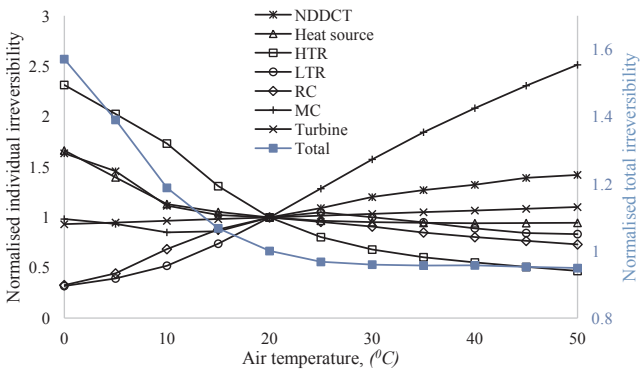

Fig. 15. Variation of irreversibility of each component of the power block. The values are normalized at 20 °C.

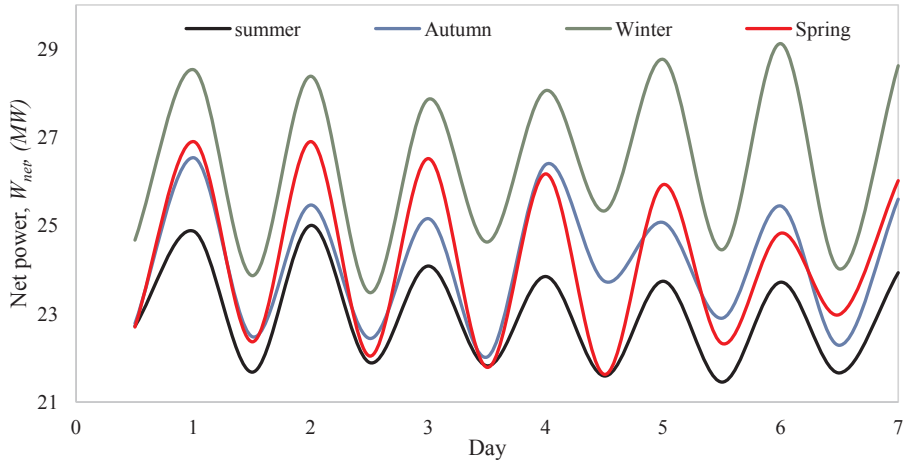

Fig. 16. Seasonal W_{net} variation in Alice Spring, NT, Australia.

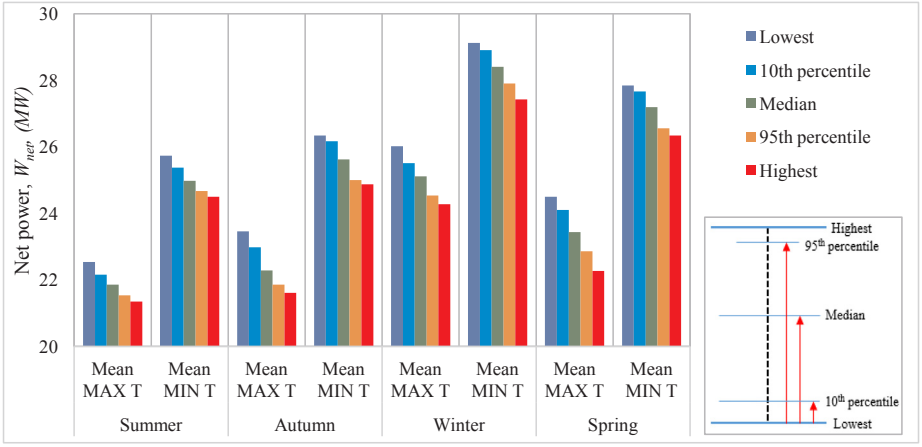

Fig. 17. Seasonal W_{net} variation based on mean maximum and minimum temperature data.

NDDCT significantly affects the cycle performance. Section 6.1 demonstrates how the NDDCT and the cycle performance are influenced by the variation of ambient condition. The irreversibility analysis is conducted and Table 5 shows the component-wise irreversibility equation. Table 6 lists the seven performance indicators used to evaluate the plant seasonal performance using the historical temperature data.

6. Results

6.1. Cycle performance coupled with detailed NDDCT model

Fig. 10(a) demonstrates the cycle performance at various ambient air temperature. The W_{net} reaches 29 MW at 0 °C air temperature and decreases with air temperature. The compression work, W_C enhances from 4.9 MW to 13.5 MW. The W_{MC} increases from 20 °C onwards and W_{RC} initially increases with air temperature and then merely decreases. The variation of mass flow rate of the two fluid streams in the NDDCT system is shown in Fig. 10(b). The M_a almost linearly drops with air temperature according to the fundamentals of cooling tower whereas the sCO_2 mass flow rate in the heat exchanger varies throughout the range of air temperature. Fig. 10(c) shows the normalized values of energy transfer in the heat exchanger and cooling tower. The Q_{HTR} decreases from 123.1 MW to 84 MW and Q_{LTR} decreases from33.2 MW to 29.5 MW. The Q_{NDDCT} varies between 29.5 MW and 23.4 MW and $Q_{heat\text{-}source}$ decreases from 60.7 MW to 44 MW. Fig. 10(d) reveals the exergy efficiency $\eta_{E,}$ thermal efficiency η variation with air temperature. Both η_E and η are maximum at the design point condition. According to Carnot theorem, the lower the heat sink temperature, the higher the cycle efficiency. However, this is not the case for super critical power cycles in which the occurrence of the cooling process takes place in the vicinity of the pseudocritical condition. The wild variation of transport properties (especially isobaric heat capacity and fluid density) near or below the pseudocritical temperature make it unique from other power cycles where the working condition of cycle fluid is under critical parameters. At 20 °C, the CIT is close to 33 °C and the rise in air temperature significantly reduces the cycle performance due to the acquirement of higher CIT values.

6.2. Examination inside the recuperators

The pinch point constraint is set at the recuperators during cycle modelling. In general, the recompression cycle with two recuperators overcomes the common pinch point phenomenon of regenerative Brayton cycle. Our code continuously checks the pinch point formation in all the heat exchangers (recuperators, NDDCT, and primary heat exchanger). The result approves no degradation of pinch point constriction in any power block components. Fig. 11 demonstrates the internal temperature profile in the two recuperators. As discussed, no occurrence of pinch point degradation arises in the recuperators. These profiles are shown at the design condition of NDDCT. However, for other working conditions, similar temperature profiles are observed in the recuperators.

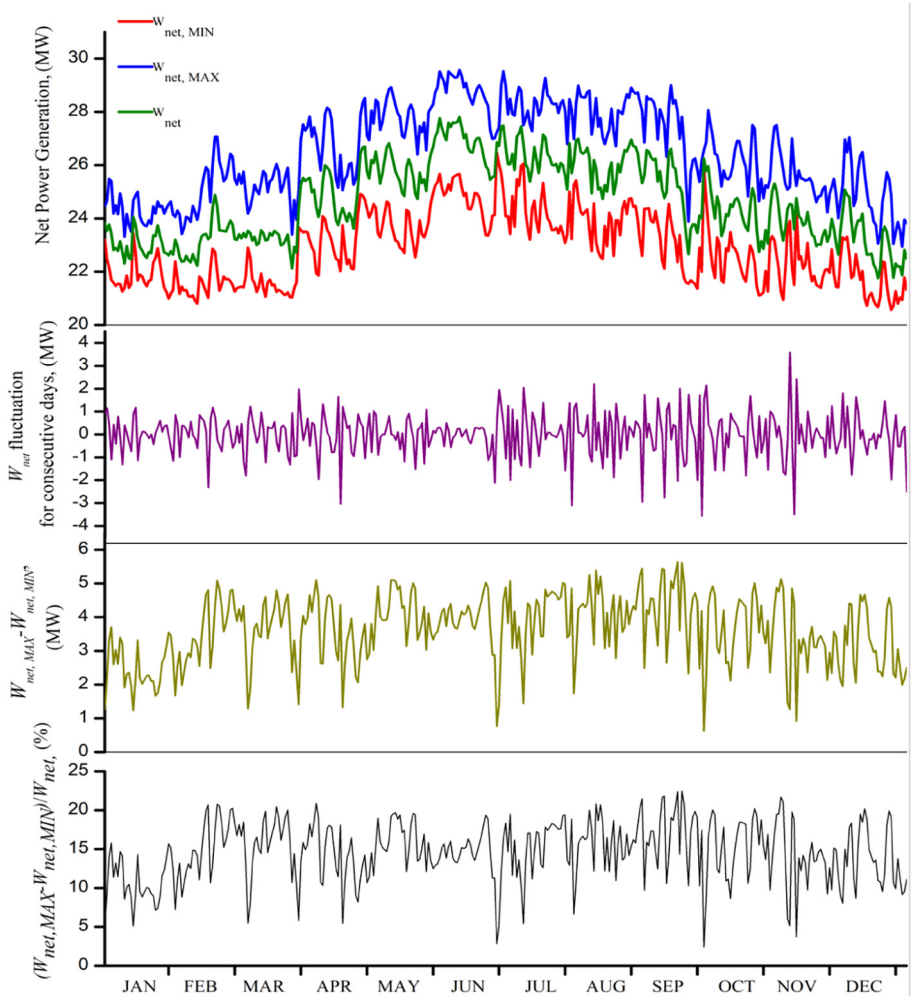

Fig. 18. Annual thermal performance in terms of $W_{net,}$ $W_{net,MIN,}$ $W_{net,MAX,}$ and variation for the consecutive days.

6.3. Examination inside the air-cooled heat exchanger

The implementation of the nodal approach in the air-cooled heat exchanger allows the visualization of the sCO_2 local heat transfer coefficient and the change of bulk temperature along the length. As the bulk temperature gradually decreases, it takes a peak value of 9.1 kW/m^2K in the tube location of $x/L = 0.8$ once the cycle fluid reaches to its pseudocritical temperature, as depicted in Fig. 12(a). The profiles are portrayed here under the design condition in which the cycle minimum temperature is 33 °C delivered by the cooling tower working under 20 °C air temperatures. For higher surrounding temperature cases, higher CITs are observed with similar sCO_2 bulk temperature profile. However, the h_s profile never takes a peak for higher CIT values since the pseudocritical temperature is never reached. The pinch point in the air-cooled heat exchanger and sCO_2 local pressure drop are shown in Fig. 12(b). At the entrance of the tube, the bulk temperature is higher for which the Reynolds number is higher due to lower fluid density and viscosity. This higher Reynolds number implies a higher pressure drop at the inlet and then gradually decreases.

6.4. Cooling tower performance

Fig. 13(a) portrays the increase of cycle fluid entrance and exit temperature and air outlet temperature inside the NDDCT. Increasing the surrounding temperature increases the entrance temperature of sCO_2 inside the tower. This is due to maintaining the constraints and boundary conditions in the simulation. Fig. 13(b) demonstrates the variation of parameters to determine the cooling potential of NDDCT. The tower range augments due to the rise of sCO_2 entrance temperature and the approach of the tower decreases with air temperature. The *ITD* of the tower increases due to the rise of both inlet temperature of air and cycle fluid inside the tower. Although, the cooling efficiency, η_C increases due to an increase in tower range, the improvement is not beneficial since the cycle performance is lower at higher ambient temperature.

6.5. Exergetic analysis

Fig. 14 shows the variation of heat input, cooling duty, and exergy input the system. At higher air temperature, the thermal energy input to the cycle decreases, as a result, the exergy input also declines from 39.1 MW to 27.2 MW. The exergy input is a decreasing function of surrounding temperature, since the sCO_2 inlet temperature of PHE increases for accomplishing the same cycle highest temperature. Fig. 15 shows the variation of the normalized value of component-wise irreversibility. The heat source, the HTR, and the NDDCT comprise most of the irreversibilities in the system. In the tower, the rise in air temperature increases the exergy input to the tower due to increase in entrance temperature of sCO_2. The exergy received by air shows minimal impact hence, the irreversibility of NDDCT gradually rises. The total exergy destruction of the cycle initially decreases sharply from 16.2 MW to 10.1 MW and then shows almost no change from 25 °C air temperature onwards. At higher surrounding temperature, the system requires lesser exergy input, hence, the total irreversibility of the

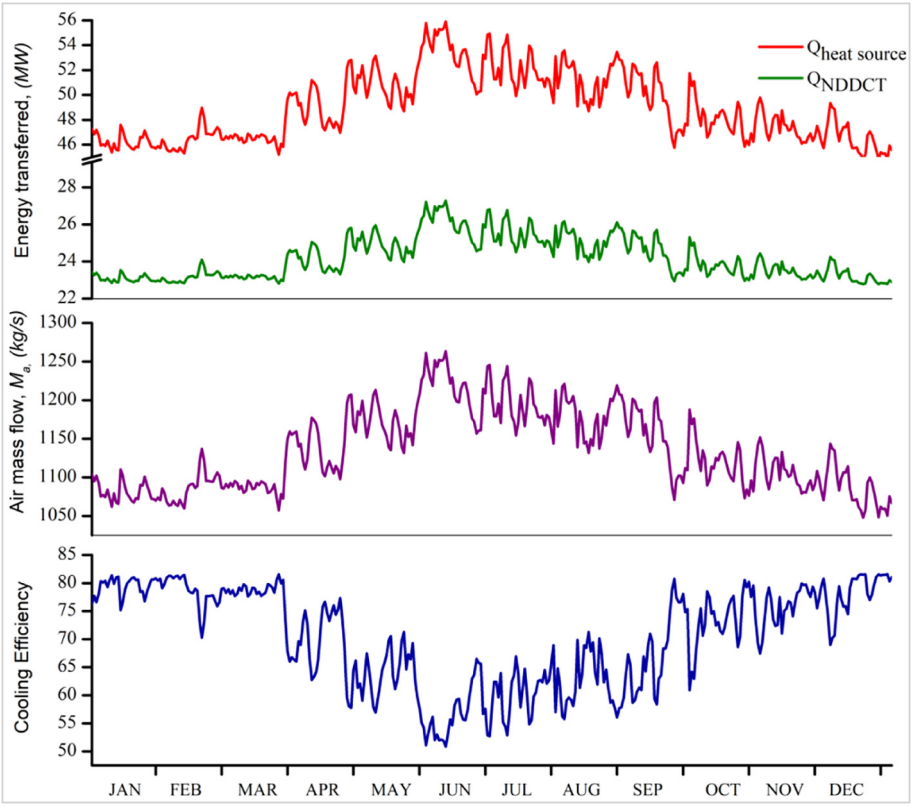

Fig. 19. Year-round NDDCT thermal performance.

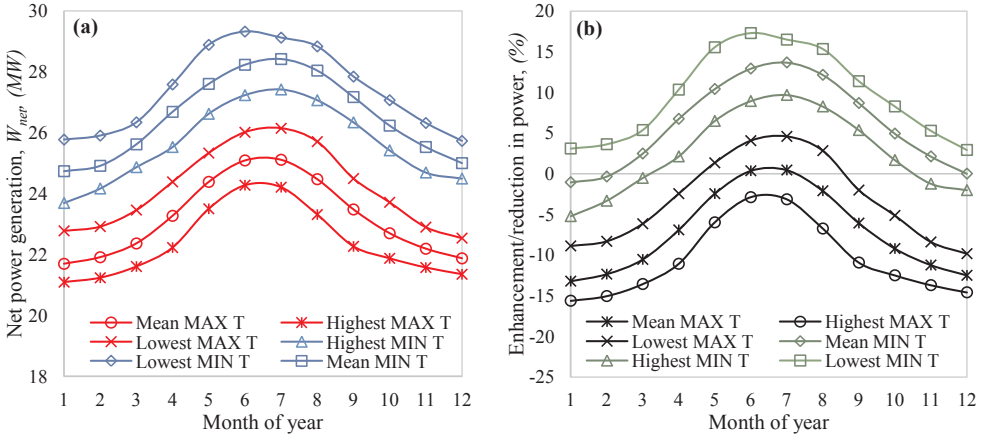

Fig. 20. Month-wise W_{net} variation with respect to various temperature data.

system decreases.

6.6. Seasonal variation affecting plant performance

Seasonal variation of the net power generated is investigated by using the meteorological data collected in Alice spring, NT 23.70S, 133.880E, Australia for NDDCT performance prediction. Sample data of daily temperature is taken from the second week of each season (December, March, June, and September), as shown in Fig. 16. Significant variation in W_{net} is observed at various seasonal conditions. In winter, the W_{net} is in the range of 25.7 MW to 27.1 MW, whereas in summer, the range is 22.7 MW to 23.7 MW at the beginning of the week and 23.9 MW to 22.7 MW at the end of the week. The lowest W_{net} of 21.4 MW is observed in summer and the maximum of 29.1 MW in winter. The average W_{net} in summer, autumn, winter, and spring are 22.9 MW, 24.1 MW, 26.4 MW, and 24 MW respectively. For a 25 MW power plant, the fluctuation in W_{net} in summer is −14.8% to −0.5%, for autumn −11.9% to +5.5%, for winter −6.1% to +16.4% and for spring −13.4% to +7.6% for the sample temperature data.

The monthly seasonal W_{net} variation with respect to mean maximum and minimum temperature data is portrayed in Fig. 17 for the month of December, March, June, and September respectively. The mean values are represented with various temperature statistics as shown in the figure. Five different temperature datasets are used to represent system performance. From *lowest* to *highest* the temperature is an increasing function. The plant performance delivers its thermal performance in accordance with the temperature profile. The deteriorated performance is observed during summer season followed by the autumn and spring season. The highest W_{net} of 29.12 MW is observed with the lowest temperature of mean minimum temperature data during the winter

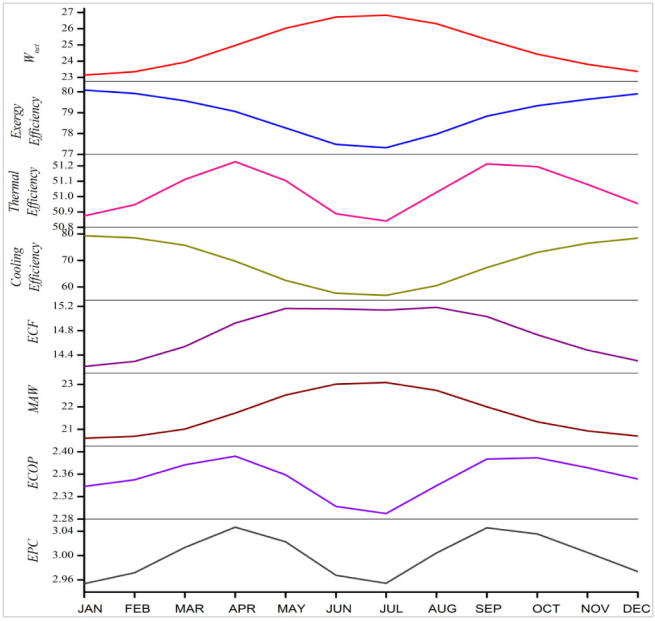

Fig. 21. Evaluation of various performance indicators.

season. The lowest value is 21.35 MW measured at the highest temperature of mean maximum temperature data during the summer season.

6.7. Annual performance Evaluation

The annual thermal performance of the power cycle using the daily maximum and minimum temperature data of 2018 in Alice Spring, NT is shown in Fig. 18. The average net power generation, W_{net} is 24.66 MW which corresponds to 50.9% of cycle efficiency. The significant variation of W_{net} is observed on a daily basis as well as on a monthly basis. In general, the W_{net} gradually increases for the period of January to June and for the rest of the months of the year, it decreases. The plant performance is significantly higher during the winter season especially in the months of June and July. The fluctuation of W_{net} for the consecutive days is also demonstrated. The plant performance variation is more dominant in the period of July to November. The maximum fluctuation for the consecutive day is 3.55 MW. The average of $(W_{net,MAX}\text{-}W_{net,MIN})$ throughout the year is 3.62 MW, the highest range is 5.63 MW (22.4%) and the lowest range is 0.63 MW (2.4%). The frequent variation of cooling tower exit temperature highly influences the overall system performance.

In Fig. 19, the variation of thermal energy supplied to the primary heat exchanger, $Q_{heatsource}$, heat rejected by the NDDCT, Q_{NDDCT}, air mass flow rate M_a and cooling tower efficiency is demonstrated. In general, both the $Q_{heatsource}$ and Q_{NDDCT} increase until the halfway of the year and then decreases for the rest of the period. The year-round variation of ambient air temperature also changes the M_a in the tower. The average M_a, $Q_{heatsource}$, and Q_{NDDCT} are 1134 kg/s, 48.96 MW and 24.17 MW respectively. The significant variation in cooling efficiency is also observed. As discussed before, the cooling efficiency is comparatively higher at higher air temperature, hence the NDDCT cooling efficiency is higher at the beginning and end of the year.

The above discussion on the plant annual performance with the variation in air temperature is for a specific year and does not necessarily represent the maximum range of thermal performance. Hence, in Fig. 20, the variation of plant performance is demonstrated using the historical temperature data (1941 to 2018). Six different temperature datasets are used to observe the month-wise plant performance. During summer (December to February) season, the W_{net} fluctuates in the range of 25.7 MW to 21 MW which corresponds to +2.9% to −15.6% of 25 MW thermal output. During autumn (March to May) season, the W_{net} varies in between 28.8 MW and 21.6 MW corresponds to +15.54% to −13.5%. During spring (September to November) season, the W_{net} changes in the range of 27.8 MW to 21.5 MW corresponds to +11.3% to −13.7%. Finally, during winter (June to August) season, the W_{net} shows the highest value of 29.3 MW corresponds to 17.3% power improvement and the lowest W_{net} is 23.3 MW corresponds to only 6.7% power reduction. The maximum range of W_{net} is 7.2 MW observed during the autumn season and the lowest range is 4.7 MW in the summer season.

6.8. Evaluation of various performance indicators

The temperature data for the period of 1941 to 2018 is also used to evaluate the various cycle performance indicators using the mean air temperature of each month. In Fig. 21, the cycle performance is investigated by evaluating different performance indicators. The W_{net} is higher in the period of June and July and fluctuates in the range of 23.1 MW to 26.8 MW. The mean year-round W_{net} is 24.85 MW. The cycle exergy efficiency is higher at the beginning and at the end of year fluctuates in the range of 77.3% to 80%. The cycle thermal efficiency varies in the range of 50.8% to 51.2%. The NDDCT cooling efficiency shows a similar trend of exergy efficiency. The ecological function criteria, *ECF* and maximum available work, *MAW* vary in the range of 14.2–15.1 MW and 20.5–23 MW respectively. The ecological coefficient of performance, *ECOP* shows the highest values in the month of April and September. The exergetic performance criteria, *EPC* shows a similar trend with *ECOP*.

7. Conclusion

An exhaustive model of the dry cooling system is developed and integrated with the sCO_2 power cycle. Prior to the modelling of the cooling system, the optimum working condition is rectified. This work comprehensively investigates the thermal performance of dry-cooled sCO_2 power cycle under variant working condition The exclusive findings are summarised below.

a) The NDDCT is modelled based on the optimum cycle minimum temperature. The influence of ambient air temperature in NDDCT is investigated under various seasonal conditions. Both the cycle efficiency and the W_{net} decrease with the increase in the surrounding temperature.
b) The seasonal performance of the cooling tower and power cycle is performed by considering the daily maximum and minimum temperature datasets. Significant variation of W_{net} is observed in various seasonal conditions. The mean W_{net} in the summer and winter are 22.9 MW and 26.4 MW respectively. The average year-round net power generation is 24.66 MW which provides a cycle efficiency of 50.9% for a specific year. The fluctuation of W_{net} for the consecutive days is investigated in absolute value as well as in percentage.
c) The variation of thermal energy input to the cycle and heat rejected by the NDDCT is also observed. In general, both the Q_{in} and Q_{NDDCT} increase until the end of the half-year and then decrease for the rest of the period. The change of air mass flow rate inside NDDCT at various ambient temperature is also revealed.
d) The month-wise and annual performance variation of the proposed power plant is also investigated. The overall plant performance is evaluated by various performance indicators using the historical mean temperature data.

Since the solar data was not included in the power plant simulation, the future work will integrate the solar tower model (heliostat field with central receiver) with dry cooled supercritical CO_2 power cycle equipped with thermal energy storage. The influence of variant solar irradiation and fluctuation of air temperature on the cooling of NDDCT

and net power generation will be investigated. The future research will demonstrate the comprehensive working mechanism of the complete system for dispatchable electricity generation.

Declaration of Competing Interest

None.

Acknowledgment

The authors thank the University of Queensland (UQ) for providing the Research Training Program scholarship. This research is conducted under the Australia Solar Thermal Research Initiative (ASTRI), a project supported by the Australia Government, through the Australia Renewable Energy Agency (ARENA).

Appendix A. Supplementary data

Supplementary data to this article can be found online at https://doi.org/10.1016/j.enconman.2019.111865.

References

[1] Garg P, Kumar P, Srinivasan K. Supercritical carbon dioxide Brayton cycle for concentrated solar power. J Supercrit Fluids 2013;76:54–60.
[2] Dostal V, Hejzlar P, Driscoll MJ. High-performance supercritical carbon dioxide cycle for next-generation nuclear reactors. Nucl Technol 2006;154(3):265–82.
[3] Dostal V, Hejzlar P, Driscoll MJ. The supercritical carbon dioxide power cycle: comparison to other advanced power cycles. Nucl Technol 2006;154(3):283–301.
[4] Osorio JD, Hovsapian R, Ordonez JC. Dynamic analysis of concentrated solar supercritical CO_2-based power generation closed-loop cycle. Appl Therm Eng 2016;93:920–34.
[5] Ehsan MM, Duniam S, Li J, Guan Z, Gurgenci H, Klimenko A. Effect of cooling system design on the performance of the recompression CO_2 cycle for concentrated solar power application. Energy 2019.
[6] Besarati SM, Goswami DY. Analysis of advanced supercritical carbon dioxide power cycles with a bottoming cycle for concentrating solar power applications. J Sol Energy Eng 2014;136(1):010904.
[7] Duniam S, Jahn I, Hooman K, Lu Y, Veeraragavan A. Comparison of direct and indirect natural draft dry cooling tower cooling of the sCO_2 Brayton cycle for concentrated solar power plants. Appl Therm Eng 2018;130:1070–80.
[8] Li X, Xia L, Gurgenci H, Guan Z. Performance enhancement for the natural draft dry cooling tower under crosswind condition by optimizing the water distribution. Int J Heat Mass Transf 2017;107:271–80.
[9] Guan Z, Hooman K, Gurgenci H. Dry cooling towers for geothermal power plants. Altern Energy Shale Gas Encycl 2016:333–49.
[10] Ehsan MM, Wang X, Guan Z, Klimenko A. Design and performance study of dry cooling system for 25 MW solar power plant operated with supercritical CO 2 cycle. Int J Therm Sci 2018;132:398–410.
[11] Cheng L. Evaluation of correlations for supercritical CO_2 cooling convective heat transfer and pressure drop in macro-and micro-scale tubes. Int J Microscale Nanoscale Therm Fluid Transport Phenom 2014;5(2):113.
[12] Ehsan MM, Guan Z, Klimenko A. A comprehensive review on heat transfer and pressure drop characteristics and correlations with supercritical CO_2 under heating and cooling applications. Renew Sustain Energy Rev 2018;92:658–75.
[13] Dang C, Hihara E. In-tube cooling heat transfer of supercritical carbon dioxide. Part 1. Experimental measurement. Int J Refrig 2004;27(7):736–47.
[14] Ma Y, Liu M, Yan J, Liu J. Thermodynamic study of main compression intercooling effects on supercritical CO_2 recompression Brayton cycle. Energy 2017;140:746–56.
[15] Deng S, Wang R, Dai Y. A comparative analysis on experimental performance of CO_2 trans-critical cycle. HVAC&R Research 2014;20(5):532–44.
[16] Conboy T, Wright S, Pasch J, Fleming D, Rochau G, Fuller R. Performance characteristics of an operating supercritical CO_2 Brayton cycle. J Eng Gas Turbines Power 2012;134(11):111703.
[17] Wang K, Li M-J, Guo J-Q, Li P, Liu Z-B. A systematic comparison of different S-CO_2 Brayton cycle layouts based on multi-objective optimization for applications in solar power tower plants. Appl Energy 2018;212:109–21.
[18] Kim S, Cho Y, Kim MS, Kim M. Characteristics and optimization of supercritical CO_2 recompression power cycle and the influence of pinch point temperature difference of recuperators. Energy 2018.
[19] Luu MT, Milani D, McNaughton R, Abbas A. Advanced control strategies for dynamic operation of a solar-assisted recompression supercritical CO_2 Brayton power cycle. Appl Therm Eng 2018.
[20] Cheng W-L, Huang W-X, Nian Y-L. Global parameter optimization and criterion formula of supercritical carbon dioxide Brayton cycle with recompression. Energy Convers Manage 2017;150:669–77.
[21] Garg P, Srinivasan K, Dutta P, Kumar P. Comparison of CO2 and steam in transcritical Rankine cycles for concentrated solar power. Energy Procedia 2014;49:1138–46.
[22] Turchi CS, Ma Z, Neises TW, Wagner MJ. Thermodynamic study of advanced supercritical carbon dioxide power cycles for concentrating solar power systems. J Sol Energy Eng 2013;135(4):041007.
[23] Iverson BD, Conboy TM, Pasch JJ, Kruizenga AM. Supercritical CO_2 Brayton cycles for solar-thermal energy. Appl Energy 2013;111:957–70.
[24] Persichilli M, Kacludis A, Zdankiewicz E, Held T. Supercritical CO2 power cycle developments and commercialization: why sCO_2 can displace steam ste. Power-Gen India & Central Asia 2012.
[25] Zeyghami M, Khalili F. Performance improvement of dry cooled advanced concentrating solar power plants using daytime radiative cooling. Energy Convers Manage 2015;106:10–20.
[26] Padilla RV, Too YCS, Beath A, McNaughton R, Stein W. Effect of pressure drop and reheating on thermal and exergetic performance of supercritical carbon dioxide Brayton cycles integrated with a solar central receiver. J Sol Energy Eng 2015;137(5):051012.
[27] Padilla RV, Too YCS, Benito R, Stein W. Exergetic analysis of supercritical CO2 Brayton cycles integrated with solar central receivers. Appl Energy 2015;148:348–65.
[28] Ho CK, Carlson M, Garg P, Kumar P. Technoeconomic analysis of alternative solarized s-CO2 Brayton cycle configurations. J Sol Energy Eng 2016;138(5):051008.
[29] Milani D, Luu MT, McNaughton R, Abbas A. Optimizing an advanced hybrid of solar-assisted supercritical CO2 Brayton cycle: a vital transition for low-carbon power generation industry. Energy Convers Manage 2017;148:1317–31.
[30] Li L, Ge Y, Luo X, Tassou SA. Experimental investigation on power generation with low grade waste heat and CO_2 transcritical power cycle. Energy Procedia 2017;123:297–304.
[31] Luu MT, Milani D, McNaughton R, Abbas A. Dynamic modelling and start-up operation of a solar-assisted recompression supercritical CO_2 Brayton power cycle. Appl Energy 2017;199:247–63.
[32] Ehsan MM, Guan Z, Klimenko A, Wang X. Design and comparison of direct and indirect cooling system for 25 MW solar power plant operated with supercritical CO_2 cycle. Energy Convers Manage 2018;168:611–28.
[33] S. IPSEpro, “Process Simulation Environment (PSE),” Simtech, Austria, 2003.
[34] Kröger DG. Air-cooled heat exchangers and cooling towers. PennWell Books 2004.
[35] Yoon SH, Kim JH, Hwang YW, Kim MS, Min K, Kim Y. Heat transfer and pressure drop characteristics during the in-tube cooling process of carbon dioxide in the supercritical region. Int J Refrig 2003;26(8):857–64.